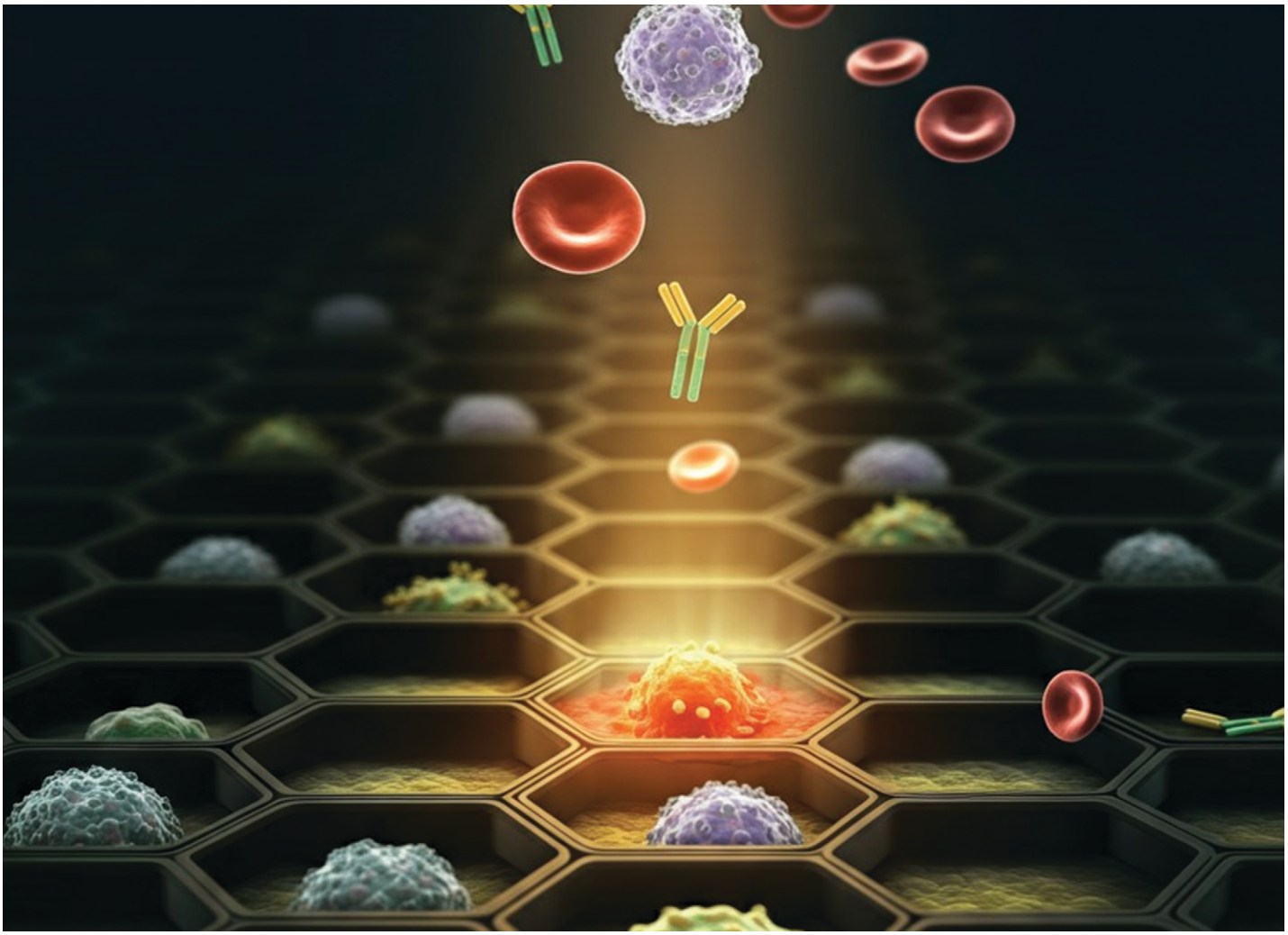

Showcasing research from Bosch Corporate Sector Research and Advance Engineering (CR, Renningen) and Professor Zengerle's laboratory in the Department of Microsystems Engineering (IMTEK) at the University of Freiburg, Germany.

Highly efficient isolation and multistep analysis of tumor cells from whole blood

Efficient on-chip isolation and analysis of tumor cells in blood samples was achieved using a microfluidic device. The core element was a silicon microcavity array with a novel decanting method, resulting in high precision and minimal cell loss, promising for point-of-care applications (image generated with Google Gemini 1.5 Pro).

Image reproduced by permission of Michael Knapp from from *Lab Chip*, 2025, **25**, 1938.

As featured in:

See Michael Knapp *et al.*, *Lab Chip*, 2025, **25**, 1938.

ROYAL SOCIETY OF CHEMISTRY

rsc.li/loc

Registered charity number: 207890

Lab on a Chip

PAPER

View Article Online
View Journal | View Issue

Cite this: *Lab Chip*, 2025, **25**, 1938

Highly efficient isolation and multistep analysis of tumor cells from whole blood†

Michael Knapp, *[ab] Samir Kadić, [b] Astrid Lux, [b] Nils Paust, [ac] Roland Zengerle[ac] and Jochen Hoffmann[b]

We present a microfluidic solution for improved tumor cell analysis based on selection-free isolation of nucleated cells from whole blood. It consists of a high-density silicon microcavity array combined with the novel fluidic strategy of microfluidic decanting. This enables multistep on-chip staining protocols comprising sample loading–blocking–extracellular staining–fixation–permeabilization and intracellular staining to quantify tumor cells. The performance of the workflow was investigated and proven by spiking colon cancer cell lines into whole blood for the detection of the epithelial tumor markers EpCAM and cytokeratin. Total cell recovery rates of ≥95% were achieved for different sample species. The method allows for rapid reagent exchange within 10 s each almost without cell loss compared to approximately 50% cell loss in reference centrifugal processing. The isolation of nucleated cells resulted in a high intra-assay precision with a CV of 2% and a single cell per well distribution of 90%, which is consistent with the theoretical estimate using Poisson statistics. The linearity of the method was demonstrated over three orders of magnitude with r^2 = 0.9998. These results demonstrate a highly efficient approach for the quantification of tumor cells from whole blood that could be integrated into automated point-of-care devices in the future.

Received 12th September 2024,
Accepted 19th February 2025

DOI: 10.1039/d4lc00759j

rsc.li/loc

Introduction

Circulating tumor cells (CTCs) are the seeds of metastasis responsible for most cancer-related deaths.[1,2] Quantification and characterization of CTCs holds great potential for early detection of metastasis, individualized tumor therapy, and therapy monitoring.[3,4] The rarity and heterogeneity of CTCs compared to non-tumor cells present in the bloodstream is a significant challenge. One milliliter of blood contains approximately 1–10 CTCs compared to 10^9 non-tumor cells.[5–7] Various methods have been developed to isolate CTCs from whole blood, most of them applying either selective enriching of CTCs or depletion of non-tumor cells.[8]

One approach is to use positive enrichment methods that target specific cell surface markers, such as epithelial cell adhesion molecule (EpCAM), which was mainly established by the FDA-approved method CellSearch®. This involves identification of cells through a semi-automated process using anti-EpCAM magnetic particles and labeling the nuclei, cytokeratins, and CD45. The typical CellSearch® CTC is defined as EpCAM+, DAPI+, cytokeratin+ and CD45−. Multiple studies have demonstrated a correlation between CTC count and clinically relevant outcomes.[5] However, several studies have also shown that this and similar systems may miss tumor cells with low EpCAM expression, such as cells that underwent epithelial–mesenchymal transition (EMT).[6,9,10]

Other systems utilize methods such as size-based or deformability-based filtration,[11–14] sedimentation or cell seeding onto flat substrates,[15–17] density-gradient centrifugation,[16] or a combination of these approaches.[18] Besides the initial isolation of only a subpopulation of tumor cells, minimizing the processing cell loss during staining and further analysis is key. The Epic Sciences system isolates cells without relying on specific size or surface marker characteristics by spreading them onto glass slides for fixation and subsequent processing. On-chip staining for multiple markers, including EpCAM, cytokeratin and CD45 is also possible as well as single-cell picking and further downstream analysis.[15,19] In the maintrac® method, tumor cells are defined as living EpCAM+ cells and are identified through simple staining and sedimentation into a microtiter plate, aiming to minimize selection bias and cell loss during processing. This method results in two to three orders of magnitude higher EpCAM+ putative tumor cells than CellSearch®, but without additional Cytokeratin or CD45 staining or genetic proof of tumorigenic origin.[20,21] The

[a] *Department of Microsystems Engineering – IMTEK, University of Freiburg, Georges-Koehler-Allee 103, 79110 Freiburg, Germany*
[b] *Robert Bosch GmbH, Corporate Sector Research and Advance Engineering, Robert-Bosch-Campus 1, 71272 Renningen, Germany.*
E-mail: michael.knapp6@de.bosch.com
[c] *Hahn-Schickard, Georges-Koehler-Allee 103, 79110 Freiburg, Germany*
† Electronic supplementary information (ESI) available. See DOI: https://doi.org/10.1039/d4lc00759j

Parsortix® system has recently received FDA clearance for automated enrichment of CTCs using a combination of filtration based on size and deformability.[22] This separation method is not limited to high EpCAM expression and can also enrich EMT cells and other phenotypes. On-chip staining is possible within the system, but imaging of the slides requires a separate device.

Several researchers utilize microwells for cell separation, allowing for a high density of individual compartments on a small device footprint. This spatial separation enables the recognition of single cells without interference from neighboring cells, simplifying imaging and downstream analysis. Swennenhuis *et al.* developed a microwell-aided filtration chip with 6400 microwells, each 70 μm in diameter featuring a 5 μm diameter pore at the bottom of each microwell on a 10 × 10 mm silicon chip. This allows for the isolation of pre-stained or pre-enriched cells into each microwell, resulting in high single-cell occupancy and subsequent single-cell isolation possibility.[23] Microwell-aided filtration devices can also directly isolate tumor cells from whole blood using a 9 μm pore with subsequent staining of cells on the chip, as demonstrated by Hosokawa *et al.*[24] However, studies have shown that there can be significant differences in size between model samples and real patient samples, suggesting that filtration approaches may result in the loss of non-standard CTCs.[7] The Sievewell® slides address this issue by integrating two 2 μm pores at the bottom of each of the 370 000 microwells, allowing buffer to pass through but not white blood cells or tumor cells. This results in a high single-cell isolation rate of 91% and on-chip staining capabilities with high total cell recovery rates of 94% in spike-in experiments.[25]

In order to facilitate routine counting of CTCs in point-of-care settings, it is necessary to develop closed systems that can handle all the steps involved in sample processing, data acquisition, and evaluation. To address this need, Loutherback and Dietz have designed a device that consists of microwells connected to a narrow channel, in which magnetically labeled cells are attracted by magnetic force and captured within the microwells.[26] Once captured, the device can be flipped, allowing for continuous exchange of the fluid above the microwells while the cells stay in place. This enables for example washing of unbound antibodies within 30 min.

While lots of novel methods were developed and optimized, none of the methods mentioned above offers a combination of (i) low loss cell isolation and processing, (ii) versatility to implement a broad range of assays as well as (iii) an integrable method into PoC devices for the quantification of tumor cells. In this study, we developed a solution for the analysis of tumor cells directly from whole blood using a high-density silicon microcavity array overcoming the mentioned limitations. This array is designed with a capacity of up to 340 000 cavities, allowing for the unbiased isolation of nucleated cells, including tumor cells. To enhance the efficiency of the system, we have implemented a novel strategy called microfluidic decanting, which enables rapid exchange of reagents within the microfluidic environment. This enables multistep on-chip staining protocols, providing a high level of flexibility in assay design for the detection of tumor cells. Because of its compact dimensions, low reagent volumes, and simple fluidic processing, our method demonstrates the potential for seamless integration into point-of-care devices.

Results & discussion

Conceptualization & microcavity array

We use an unbiased isolation approach requiring less than 100 μl of whole blood. The blood sample is diluted 1 : 5 in an erythrocytes lysis buffer and transferred to a flow cell with a

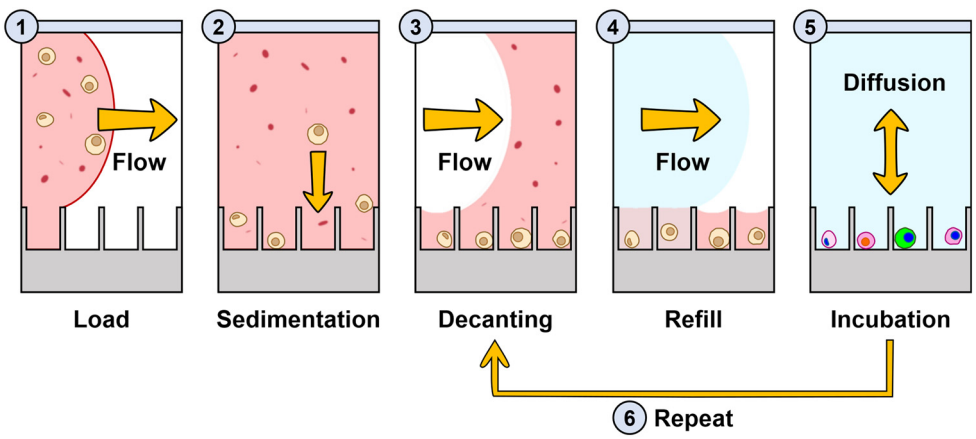

Fig. 1 Workflow of the sample processing procedure. Initially, the sample is introduced into a flow cell with a structured silicon microcavity array at the bottom of the sedimentation chamber (1). During a 20 min stationary phase, the nucleated cells in the sample sediment into the microcavities at the bottom of the chamber under the influence of gravity (2). To achieve buffer exchange and cellular staining, two methods can be employed: continuous washing with clear wash buffer (Fig. S2†) or microfluidic decanting, where the headspace volume is displaced with an immiscible air phase (3). The chamber can then be refilled (4) with the desired fluid, such as staining buffer, allowing for rapid diffusive buffer exchange in each microcavity (5). This decanting and refill process can be repeated (6) to facilitate multiple wash steps or to carry out multistep staining protocols.

structured silicon microcavity array at the bottom of the sedimentation chamber (Fig. 1.1). During a 20 min stationary phase, all nucleated cells sediment into the microcavities at the bottom due to gravitational force (2).

Buffer exchange and cellular staining can be achieved by continuous washing (Fig. S2†) or by microfluidic decanting that mimics macroscopic centrifugal processing.

The liquid volume above the microcavity array is displaced with an immiscible air phase, while the cells are retained in the microcavities due to gravitational forces and fluidic shielding from the flow in the headspace (3). The cavity and headspace geometry were designed based on simulations to ensure that they are adequately sized to fit at least one cell. Due to the large headspace of 640 μm compared to the flat cavities of 25–28 μm, the parabolic flow profile minimizes flow velocity on the bottom and prevents the flow streamlines from entering the cavities. Instead, the flow generates recirculating vortices within the cavities, thus effectively retaining the cells inside (see ESI-5.1† for simulation results). Subsequent refilling (4) of the chamber with the desired fluid (*e.g.*, staining buffer) enables rapid diffusive exchange in each microwell within a few seconds due to short diffusion lengths (5). Decanting and refill take approximately 10 s depending on the applied flow rate and can be repeated (6) to enable multiple wash steps or to perform an on-chip fixation–permeabilization–staining protocol (see ESI-Video1† for demonstration of the filling and decanting process). By optical detection and classification of the cells the count of tumor cells in the leukocytes background can be determined.

The microcavity array type 1 comprises up to 340 000 hexagonal cavities in a detection area of 12.5 mm × 12.5 mm. Each cavity has a short diagonal length d_2 = 20 μm, a depth d = 25 μm, a bar width w = 3 μm and a volume V = 8.7 pl. An image of the microcavity array type 1 is shown in Fig. 2.A. The 20 μm cavity geometries were chosen to enhance the single cell isolation, whereas a microcavity array type 2 (d_2 = 42 μm, d = 28 μm, w = 3 μm and V = 42.8 pl) was designed to also enable the isolation of larger cells and clusters.[27,28] The microcavity array was integrated into 3D-printed flow cells for controlled fluidic processing. A flow cell contains a microcavity array of type 1 or 2 and is available in two configurations (Fig. 2.B). Variant A was designed for simple and fast fluidic processing whereas variant B was designed for improved volume separation minimizing the dead volume. The sedimentation chamber inside the flow cell is the volume above the microcavity array that is used for the geometric separation of a defined detection volume of 45 μl in variant A or 100 μl in variant B. Detailed fabrication and experimental methods can be found in the ESI.†

Characterization of the cell isolation step

In order to assess the effectiveness of the sedimentation array technology in isolating all nucleated cells from whole blood without bias, we identified several analytical performance parameters. These included the initial recovery rate after sample load, the intra-assay precision, the recovery of cells during continuous reagent exchange, the assay linearity, and the distribution of cells after sedimentation. All experiments were conducted using variant B flow cells, which were specifically designed for precise volume separation, as outlined in the supplements (ESI-3.2†).

Initial recovery rate after sample load. The initial recovery rate after sample load refers to the percentage of all cells that were recovered after transferring the sample into the flow cell and sedimentation of the cells. Thus, it is a measure for the capability of the microfluidic setup for cell isolation without label dependent enrichment or depletion only depending on gravitational forces and should ideally be 100%. To determine the initial recovery rate of our method, we processed n = 6 microcavity type 1 and n = 6 type 2 flow cells and n = 3 reference samples whose cell count was defined as 100% as described in the supplements (ESI-3.4.1†). The initial recovery rate after sample load in the flow cells was 103.6 ± 2.8% (type 1, d_2 = 20 μm) and 102.7 ± 2.5% (type 2, d_2 = 42 μm), however the difference was non-significant compared to the reference. Thus, our microfluidic setup and processing is capable for the unbiased isolation of nucleated cells by sedimentation into the microcavity array. A loading rate greater than 100% can be explained by two factors: (i) slight variations in the 3D-printed parts and manual assembly of components leading to a larger volume separation, and (ii) the introduction of cells from the dead volume. However, even at this early prototype state, the use of 3D-printed parts demonstrated high reproducibility, with potential for further improvement in fabrication and fluidic processes.

Intra-assay precision. The intra-assay precision is a measure for the repeatability of an assay when performing individual measurements of the same analyte under recurring conditions. To determine intra-assay precision, we processed n = 6 microcavity type 1 and n = 6 type 2 flow cells at two different days as described in the supplements (ESI-3.4.2†). The average cell counts, and repeatability limits are displayed in Fig. 3.A. All individual measurements (see Table S.1†) fell within the corresponding repeatability range, indicating no statistically significant differences neither between the six flow cells of the same geometry nor between all twelve flow cells processed on each day and thus proofing a high intra-assay precision.

Cell recovery during continuous reagent exchange. Cell recovery during continuous reagent exchange is a parameter used to quantify the loss of cells that occurs during reagent exchange, which is necessary to achieve optical transparency and enable cell imaging. To obtain accurate and reliable results, recovery should be as high as possible, ensuring that the cell counts obtained are not affected by any systemic losses during the processing. Therefore, we evaluated the influence of different flow rates during continuous reagent exchange on the cell recovery at six flow rates (2, 5, 10, 20, 40, and 80 μl s^{-1}) as described in the supplements (ESI-

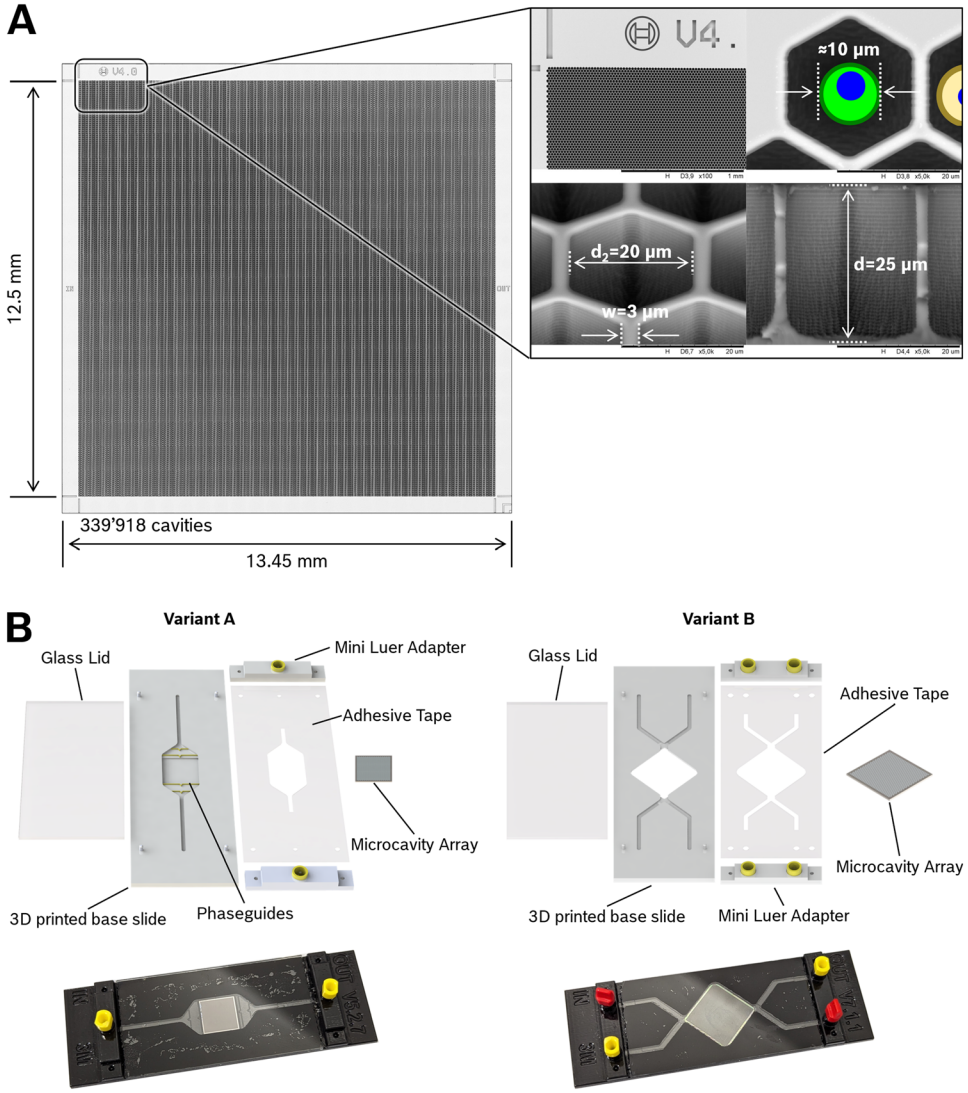

Fig. 2 Microcavity array and flow cells. A: Microscopic image of the microcavity array type 1 with approximately 340 000 cavities on 12.5 × 12.5 mm^2 detection area. B: Microfluidic integration of the microcavity array into the flow cell. The microcavity array was integrated into the 3D printed slide before the adhesive tape with Mini Luer adapters and glass lid were applied. The fluidic access was realized using a pipette or syringe pump *via* the Mini Luer adapters. Left: Variant A flow cell with horizontal sedimentation chamber and phaseguides for integration of 9 × 9 mm microcavity arrays. Right: Variant B flow cell with 45° rotated sedimentation chamber for integration of 13.45 × 13.45 mm microcavity arrays.

3.4.3†). High recovery rates exceeding 95% were achieved for each flow rate and cavity geometry (Fig. 3.B). The CV was 2.1% for 20 µm cavities and 1.8% for 42 µm cavities. There was no statistically significant difference neither within a cavity geometry as a function of the flow rate nor between the two cavity geometries, resulting in an overall recovery of 98.4 ± 2.2%. This proves that our solution exhibits high robustness across a wide range of flow rates, thus not only being suitable for processing with accurate flow control but also for simple manual processing using a pipette or LoC systems with pulsatile flow rate profiles. While higher flow rates could potentially lead to increased cell loss, exploring this was beyond the scope of the current study. The flow rates investigated here established a suitable operational range for our prototype and its intended application.

Assay linearity. Assay linearity describes the ability of the method to isolate and quantify tumor cells on the microcavity array within a large population of non-tumor cells that is directly proportional to the actual number of tumor cells introduced. Since real patient samples are likely to have varying tumor cell counts throughout the course of therapy, it should at least cover the range of 0 to 1000 cells per microcavity array, which would correspond to 0 to 50 000 tumor cells per ml whole blood.[7] To determine the assay linearity, we spiked HCT-116 cells or fluorescent beads into whole blood and processed the samples as described in the supplements (ESI-3.4.4†). Assay linearity was evaluated by plotting the number of HCTs or fluorescent beads recovered per microcavity array for each of the spike-in concentrations against the reference samples. The isolation process was

A

Sample	Mean ± SD	r	Range
20µm_d1	119262 ± 2946	10713	108550 – 129975
42µm_d1	119575 ± 2956	10749	108826 – 130325
20µm_d2	108358 ± 2938	10681	97677 – 119039
42µm_d2	110875 ± 3049	11087	99789 – 121962

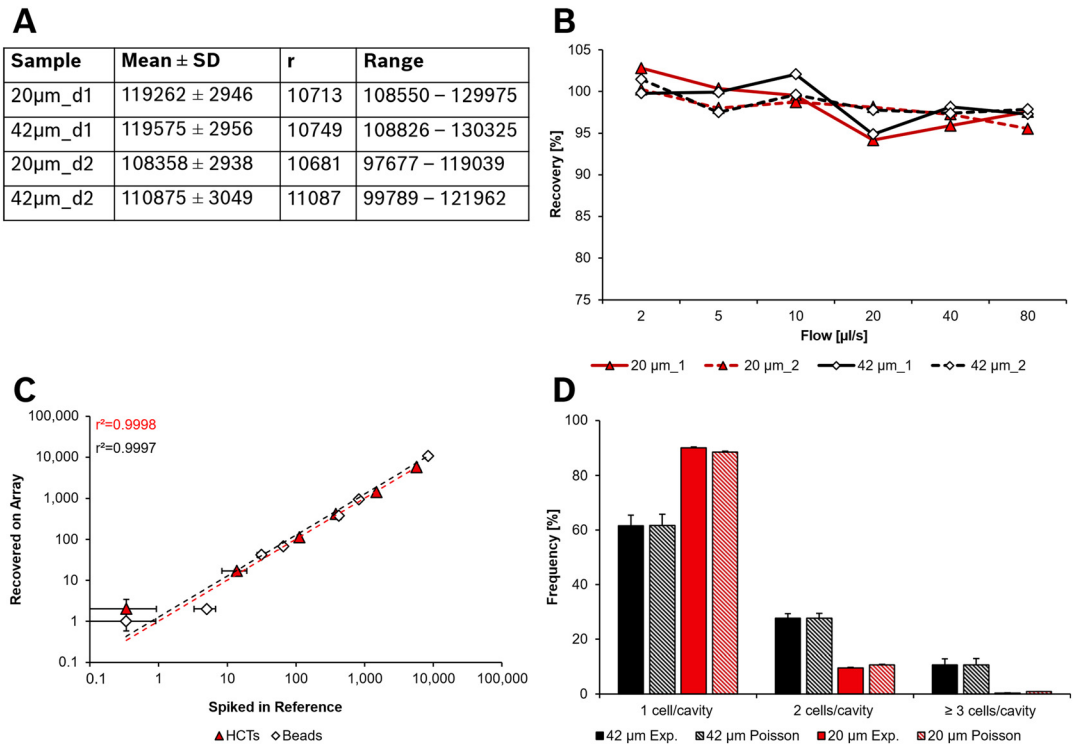

Fig. 3 Characterization of the cell isolation setup. A: Average cell counts and repeatability limits of the measurements for intra-assay precision. B: Recovery during continuous reagent exchange at defined flow rates for 20 µm (red) and 42 µm (white) cavities, each n = 2. Overall, an average recovery of 98.4 ± 2.2% was achieved. C: Assay linearity assessed by comparing the recovered HCTs (red) or beads (white) on the microcavity array to the reference. Linear regression analysis revealed high linear correlation over at least three orders of magnitude from 10–10 000 HCTs or beads with r^2 of 0.9998 and 0.9997. D: Experimentally determined cell distribution (solid) in 20 µm (red) and 42 µm (black) cavities loaded with cells *versus* theoretical estimate (dashed) using Poisson statistics, each n = 3.

shown to be linear over at least three orders of magnitude (r^2 = 0.9998 for HCTs and r^2 = 0.9997 for fluorescent beads), which makes it suitable for the analysis of both small and large numbers of tumor cells in a large background of non-tumor cells. Furthermore, no difference was observed in the detection of defined, standardized beads compared to a homogeneous mixture of HCT cells (Fig. 3.C).

Although the results demonstrate a high degree of linearity, further replicates are necessary, particularly in the range <10 cells per sample, to minimize the statistical scatter of the data and achieve reliable results.

If no spike-in was performed (0 cells or beads), no false-positive events were detected neither in the reference nor in the microcavity array (data not shown). A definite statement on the specificity of the staining must be made in further investigations on real patient samples and is beyond the scope of this study.

Cell distribution after sedimentation. The cell distribution after sedimentation describes the frequency of cavities loaded with a defined number of cells. To ensure accurate optical detection and classification of the cells, the cavities should ideally only be loaded with one cell per cavity. The sedimentation process and the theoretical cell distribution were modeled using the Poisson distribution as described in the supplements (ESI-3.4.5†). Due to the statistical nature of the distribution process, also none, two or more cells can be in one cavity. For experimental validation, n = 3 microcavity array type 1 and n = 3 type 2 flow cells were processed with an all-in-one staining and the individual cell count per array was determined to calculate the theoretical cell distribution over the whole detection area. In particular, the frequency of the events 1, 2 and ≥3 cells per cavity was investigated in cavities loaded with cells and showed no significant differences (α = 0.05) comparing the experimental with the theoretical cell distribution (Fig. 3.D). The cell distribution in all cavities including the empty ones can be found in the supplements (Fig. S5†). Using the array with smaller cavities results in a higher percentage of empty cavities (80% for 20 µm *vs.* 40% for 42 µm). This was due to the increased density of smaller cavities (~2205 cavities per mm^2 for 20 µm and ~572 cavities per mm^2 for 42 µm cavities) and is not indicative of a loss in overall capture efficiency. The difference was only in the cells/cavity distribution across the array. From this, the following hypotheses can be inferred: (i) the sample was uniformly mixed upon input into the flow cell, resulting in homogeneous sedimentation of cells across the entire detection area, and (ii) the cells sediment independently of each other, without significant clumping or interactions that would interfere with cell singulation. Additionally, it can be observed that the single-cell occupancy in 20 µm cavities was approximately 30% higher than in 42 µm cavities, which is advantageous for optical detection and classification. Based

on our data, the theoretical modeling using Poisson distribution provides a good approximation of the real conditions, allowing for a theoretical design of the optimal ratio of cells to cavities based on the desired occupancy level. Additionally, the cell distribution could be determined routinely and used as an internal process control to evaluate homogeneous mixing or successful loading of the array.

Rapid microfluidic reagent exchange

The previous findings clearly demonstrated that our solution can effectively isolate nucleated cells without selection bias, with recovery rates 95% or higher. However, these results are limited to a method where all cells are stained together before being applied to the microcavity array. This approach only allows for the discrimination of cells based on their surface antigens and on membrane permeant dyes like Hoechst 33342 or propidium iodide. Additionally, all the reagents have the same incubation time and are present in the lyse and staining mixture, which could potentially interfere with each other and not provide optimal reaction conditions, thus limiting the flexibility of potential assays. In fact, labelling of intracellular antigens would not be possible with an all-in-one staining approach, as a sequential introduction of fixation and permeabilization buffer with subsequent wash steps would be necessary.

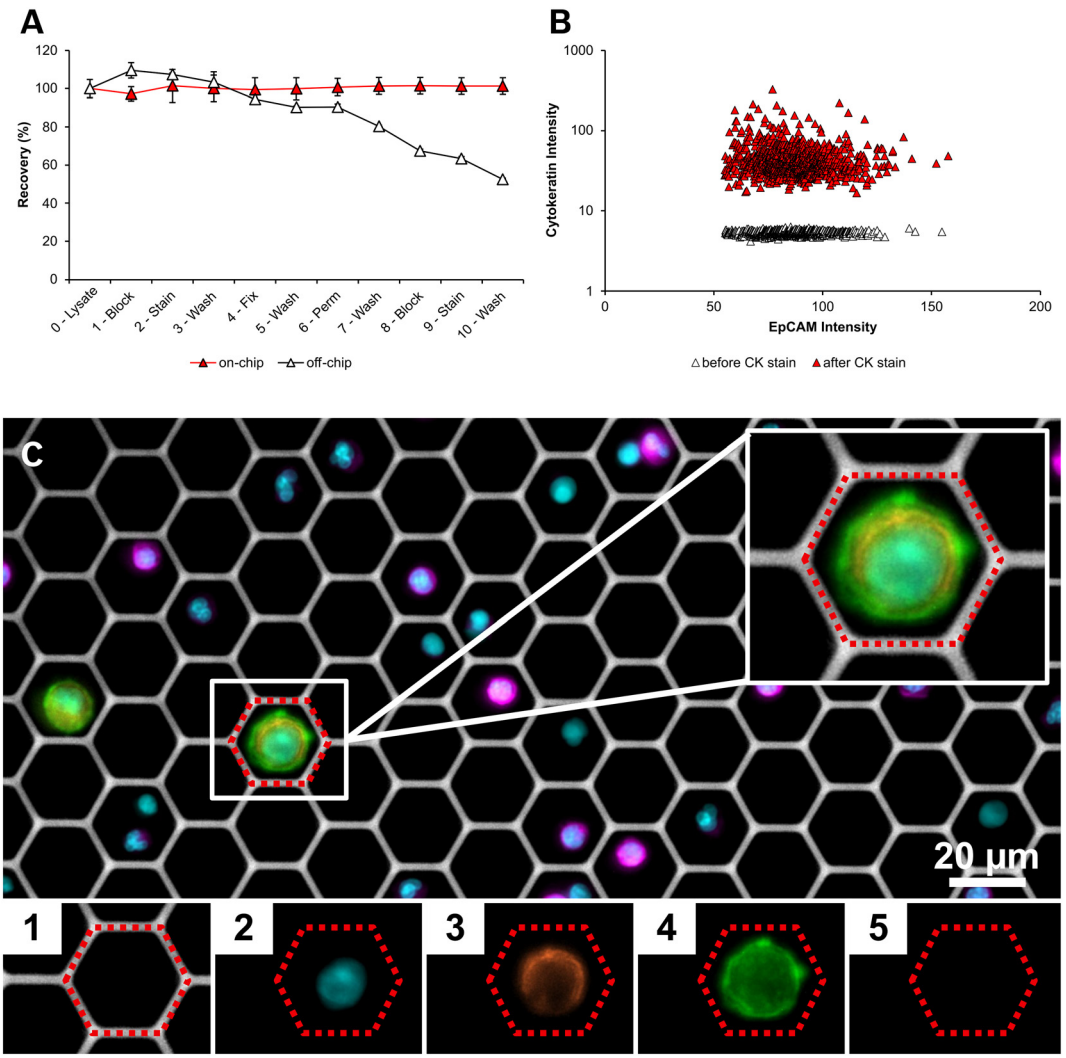

Fig. 4 Multistep staining protocols by microfluidic decanting. A: Cell recovery during intracellular staining procedure. Cells were processed either on-chip (red) with microfluidic decanting or off-chip (white) with a centrifugation protocol. Normalized to the initial cell count in the blood lysate, each n = 3. The final yields were 101.3 ± 4.4% (on-chip) and 52.5 ± 0.6% (off-chip) with an average on-chip yield of 100.4 ± 4.8% over ten reagent exchanges. B: Fluorescence intensity of cells labeled with EpCAM and cytokeratin antibodies before (white) and after (red) addition of the intracellular staining cocktail. The successful reagent exchange in the cavities can be detected by a significant signal increase in the cytokeratin channel after staining, indicating a correct intracellular antibody labeling of the cells. C: Microscopic cell detection of spiked HCT116 tumor cells in blood on the microcavity array. The cells were sequentially stained by microfluidic decanting and imaged in five detection channels. 1: Brightfield. 2: Hoechst 33342 (DAPI, nucleus stain). 3: Cytokeratin (Cy3, epithelial intracellular tumor marker). 4: EpCAM (FITC, epithelial surface tumor marker). 5: CD45 (Cy5, surface leukocyte marker). The red labeled well contained one tumor cell.

To address this limitation, we developed a process named here as microfluidic decanting, which aims to implement reagent exchanges comparable to centrifugal processing into our microfluidic solution (Fig. 1). This process enables sequential processing with defined incubation times and rapid exchange of reagents, as required in most immunohistochemical assay protocols.

To quantify cell loss during microfluidic decanting, we compared cell recovery after reagent exchange using on-chip microfluidic decanting with the off-chip reference method of centrifugation, decanting, and resuspension. The comparison was conducted in $n = 3$ microcavity type 1 variant A flow cells for simple processing using a pipette as described in the supplements (ESI-2.3†). The protocol included ten reagent exchanges, with a final yield of 101.3 ± 4.4% on-chip and 52.5 ± 0.6% off-chip (Fig. 4.A). For on-chip processing, there was no significant difference in the cell count per reagent exchange, indicating an average yield of 100.4 ± 4.8%, which was excellent compared to the approximately 50% cell loss in reference off-chip processing. This is particularly noteworthy as the highest cell losses in off-chip processing occurred after permeabilization of the cells, which is necessary for assays requiring intracellular staining of protein such as cytokeratin.

Implementation of multistep on-chip staining protocol

We further wanted to provide a universally applicable solution to isolate and stain multiple types of cells, without limitations to only surface antigens or all-in-one staining cocktails. The previous findings clearly demonstrated that cells can be processed on-chip with excellent recovery rates. We also wanted to demonstrate that we are not only able to recover individual cells during microfluidic decanting but also successfully exchange reagents within the individual cavities after refill by diffusion, which can be visualized by staining cells with *e.g.* antibodies. Therefore, we analyzed the EpCAM (FITC-channel) and cytokeratin (Cy3-channel) intensities of the HCTs in the previous experiment before and after addition of the intracellular staining cocktail (Fig. 4.B). Thus, the subset before CK stain corresponds to step no. 8-block and the subset after CK stain corresponds to step no. 10-wash. As clearly visible, the average intensity of all cells in the cytokeratin channel raised significantly from 5.3 ± 0.2 before the staining (white) to 34.9 ± 16.5 (red), which corresponds to an approximately 6.5-fold increase, underlying the successful labeling of the cells. A visual impression of the sequential on-chip staining can be found in Fig. S3.† The combination of microfluidic decanting with the microcavity array thus enables us to successfully implement highly efficient on-chip staining protocols regarding processing time, reagent consumption and cell loss with high flexibility in the choice or combination of reagents.

For optical detection, classification, and quantification of different cell populations, the microcavity arrays were imaged with a microscope as described in the supplements (ESI-3.5†). Fig. 4.C shows an exemplary overlay of 0.05% of the total detection area of one microcavity array type 1 (20 μm, 9 × 9 mm) with sedimented and on-chip stained cells in the microcavities (1, brightfield). As a universal marker for all nucleated cells, Hoechst 33342 (2, blue, DAPI channel) was used. The HCT116 tumor cells were stained with intracellular PE-labeled anti-cytokeratin (3, orange, Cy3 channel) and VioBright B515-labeled anti-EpCAM antibody (4, green, FITC channel). Additionally, leukocytes were stained with APC-labeled anti-CD45 antibody (5, magenta, Cy5 channel). By single cell detection and intensity quantification in each channel, we were able to clearly discriminate individual cells and classify into tumor cells and non-tumor cells or leukocytes as described in the supplements (Fig. S3†). The inset shows one single tumor cell isolated in a microcavity.

Conclusion & outlook

We have developed a simple solution for cell isolation and multistep on-chip analysis using a microcavity array. The method does not rely on specific surface markers for cell isolation and does not require bulky or expensive fluidic controls, thus enabling also a processing using a pipette. Approximately 98.4 ± 2.2% of the seeded cells could still be recovered after a single wash step. The method further demonstrated high linearity with a correlation coefficient (r^2) of ≥0.9997, using cell culture and bead spike-in over at least three orders of magnitude from 10–10 000 events. The cell distribution after sedimentation showed no significant differences to the theoretical estimate using Poisson statistics with a single cell occupancy of approx. 60% or 90% using the 42 μm or 20 μm cavities comparable to sieved microwells.[23,25] In the current study, we fabricated microcavity arrays with up to 340 000 cavities (type 1: $d_2 = 20$ μm) on a detection area of 156.25 mm^2. This method is easily scalable, so even larger detection areas for processing of larger volumes or other cavity diameters and depths could be realized to further optimize cell trapping efficiency.[8,27]

The theoretical estimation using Poisson distribution can be used to determine the minimum number of cavities needed for a certain cell number range that is expected for real patients. Additionally, the choice of cavity diameter is highly dependent on the cell size that is expected. When targeting single CTCs out of the blood stream, the 20 μm cavities are advantageous in case of single cell distribution. However, they will not be suitable to detect CTC clusters of two or more cells, simply because of spatial limitations.[7,28] Therefore, the larger cavities with $d_2 = 42$ μm should be used. Depending on the sample species, assay characteristics and downstream analysis, further optimization of not only the diameter but also the shape, depth and pitch of the cavities could be possible as described elsewhere.[13,26,27]

We further implemented the novel solution of microfluidic decanting, mimicking centrifugal processing in a microfluidic setup. This approach achieved high recovery rates of 100.4 ± 4.8% with minimal cell loss over ten reagent

exchanges. Currently, the experiments were manually performed using a pipette, still achieving reproducible results. However, user variability is a key factor. Depending on the fluid velocity during pipetting, potential cell losses could occur. This could easily be avoided by applying good laboratory pipetting practices, by using a syringe pump or by integration into LoC systems with controlled flow rates.

Additionally, we successfully demonstrated the labeling of intracellular cytokeratin in spiked-in cell culture, indicating the adaptability of the platform to various assay detection reagents. This makes it a versatile technology for different tumor phenotypes. Further experiments should explore the platforms versatility in assay design, including different cell lines and marker combinations. This could include variations in cell size and epithelial and mesenchymal marker expression, allowing analysis of not only the subset of EpCAM+ cells but also cells that have undergone EMT.[6,7,9]

Our study demonstrates that the combination of microfluidic sample processing and a high-density microcavity array offers a (i) low loss approach with high sensitivity for cell isolation and further processing by microfluidic decanting, (ii) thus enabling high flexibility in assay design through multistep on-chip staining possibilities. As the method was designed for a small footprint and low reagent consumption and further proved to be robust at different fluidic regimes, we are (iii) compatible to lab-on-a-chip systems like Vivalytic from Bosch Healthcare Solutions.[29] This system combines sample processing, image acquisition, and data analysis in a single device. Thus, by integration of our method into a LoC-cartridge, a fully automated workflow for the quantification of spiked tumor cells in whole blood could be implemented, overcoming the mentioned limitations of the current state of the art. However, there are still several hurdles like the influence of the microfluidics and mechanical stress to the cell characteristics which is currently unclear and must be addressed in further studies.

However, the biggest limitation now, or rather the major uncertainty, is whether the small amount of blood will be sufficient. The current assay has a limit of detection of 50 tumor cells per ml whole blood, assuming ideal processing with no cell loss. This may only be achievable if isolation-free approaches, as described in previous studies, can detect significantly higher numbers of tumor cells. Although Gold *et al.* could demonstrate a clinical correlation of their putative CTCs, the lack of genetic proof remains a significant uncertainty.[20] As the common opinion in the literature suggests a CTC count of only 1–10 CTCs ml^{-1}, our small volume approach directly from whole blood will not be suitable as described.[5,7] The next step would involve analyzing real patient data to determine the potential for isolating real CTCs. Alternatively, one could combine a selective enrichment step as described elsewhere and process only the enriched fraction with our method to minimize at least cell loss due to processing.[8] With a few adjustments, our solution could also serve as a simple and scalable lab consumable for screening different assay conditions and recovering cells using a single cell picker after staining and classification.[16,25]

Data availability

The data supporting the findings of this study are available within the article and its ESI.† Additional source data are available from the corresponding author upon reasonable request.

Author contributions

M. K. further developed the technology based on the work of S. K. and A. L.; M. K. designed and performed the experiments with advice from S. K., A. L. and J. H. under the supervision of N. P., R. Z. and J. H.; M. K. analyzed the data and wrote the manuscript. All authors reviewed the manuscript and provided scientific advice.

Conflicts of interest

The authors declare the following competing interests. Some of the aspects addressed in this article are subject of patent application by Robert Bosch GmbH.

Acknowledgements

The authors gratefully acknowledge Marvin Heyer, Matthias Ege and Jan Schlegel for their assistance with the experiments and analysis. The authors thank Luise Nagel for conducting the numerical flow simulations, providing the raw data, and assisting with the interpretation of the results. We especially thank Franz Laermer for his insightful advice, thorough proofreading, and his constant willingness to discuss the research, which proved invaluable throughout this project.

References

1 H. Dillekås, M. S. Rogers and O. Straume, *Cancer Med.*, 2019, **8**, 5574–5576.
2 D. Lin, L. Shen, M. Luo, K. Zhang, J. Li, Q. Yang, F. Zhu, D. Zhou, S. Zheng, Y. Chen and J. Zhou, *Signal Transduction Targeted Ther.*, 2021, **6**, 404.
3 *Circulating Tumor Cells: Advances in Liquid Biopsy Technologies*, ed. R. J. Cote and E. Lianidou, Springer International Publishing, Cham, 2023.
4 Z. Habli, W. AlChamaa, R. Saab, H. Kadara and M. L. Khraiche, *Cancers*, 2020, **12**, 1930.
5 S. Riethdorf, L. O'Flaherty, C. Hille and K. Pantel, *Adv. Drug Delivery Rev.*, 2018, **125**, 102–121.
6 J. F. Swennenhuis, G. van Dalum, L. L. Zeune and L. W. M. M. Terstappen, *Expert Rev. Mol. Diagn.*, 2016, **16**, 1291–1305.
7 P. A. J. Mendelaar, J. Kraan, M. Van, L. L. Zeune, L. W. M. M. Terstappen, E. Oomen-de Hoop, J. W. M. Martens and S. Sleijfer, *Mol. Oncol.*, 2021, **15**, 116–125.

8 A. J. Rushton, G. Nteliopoulos, J. A. Shaw and R. C. Coombes, *Cancers*, 2021, **13**, 970.
9 A. Genna, A. M. Vanwynsberghe, A. V. Villard, C. Pottier, J. Ancel, M. Polette and C. Gilles, *Cancers*, 2020, **12**, 1632.
10 J. Fares, M. Y. Fares, H. H. Khachfe, H. A. Salhab and Y. Fares, *Signal Transduction Targeted Ther.*, 2020, **5**, 28.
11 D. L. Adams, R. K. Alpaugh, S. S. Martin, M. Charpentier, S. Chumsri, M. Cristofanilli, D. K. Adams, O. V. Makarova, P. Zhu, S. Li, C.-M. Tang and S. Stefansson, *RSC Adv.*, 2016, **6**, 6405–6414.
12 L. S. Lim, M. Hu, M. C. Huang, W. C. Cheong, A. T. L. Gan, X. L. Looi, S. M. Leong, E. S.-C. Koay and M.-H. Li, *Lab Chip*, 2012, **12**, 4388.
13 M. Hosokawa, T. Yoshikawa, R. Negishi, T. Yoshino, Y. Koh, H. Kenmotsu, T. Naito, T. Takahashi, N. Yamamoto, Y. Kikuhara, H. Kanbara, T. Tanaka, K. Yamaguchi and T. Matsunaga, *Anal. Chem.*, 2013, **85**, 5692–5698.
14 A. Lux, H. Bott, N. P. Malek, R. Zengerle, T. Maucher and J. Hoffmann, *Biosensors*, 2021, **11**, 312.
15 S. L. Werner, R. P. Graf, M. Landers, D. T. Valenta, M. Schroeder, S. B. Greene, N. Bales, R. Dittamore and D. Marrinucci, *J. Circ. Biomarkers*, 2015, **4**, 3.
16 E. P. Kaldjian, A. B. Ramirez, Y. Sun, D. E. Campton, J. L. Werbin, P. Varshavskaya, S. Quarre, T. George, A. Madan, C. A. Blau and R. Seubert, *Cytometry, Part A*, 2018, **93**, 1220–1225.
17 K. Pachmann, J. H. Clement, C.-P. Schneider, B. Willen, O. Camara, U. Pachmann and K. Höffken, *Clin. Chem. Lab. Med.*, 2005, **43**, 617–627.
18 F. S. Iliescu, D. P. Poenar, F. Yu, M. Ni, K. H. Chan, I. Cima, H. K. Taylor, I. Cima and C. Iliescu, *Biomicrofluidics*, 2019, **13**, 041503.
19 S. Chai, C. Ruiz-Velasco, A. Naghdloo, M. Pore, M. Singh, N. Matsumoto, A. Kolatkar, L. Xu, S. Shishido, A. Aparicio, A. J. Zurita, J. Hicks and P. Kuhn, *npj Precis. Oncol.*, 2022, **6**, 41.
20 M. Gold, K. Pachmann, A. Kiani and R. Schobert, *Mol. Clin. Oncol.*, 2021, **15**, 201.
21 M. Mäurer, D. Schott, M. Pizon, S. Drozdz, T. Wendt, A. Wittig and K. Pachmann, *Curr. Oncol.*, 2022, **30**, 261–273.
22 M. C. Miller, P. S. Robinson, C. Wagner and D. J. O'Shannessy, *Cytometry, Part A*, 2018, **93**, 1234–1239.
23 J. F. Swennenhuis, A. G. J. Tibbe, M. Stevens, M. R. Katika, J. van Dalum, H. Duy Tong, C. J. M. van Rijn and L. W. M. M. Terstappen, *Lab Chip*, 2015, **15**, 3039–3046.
24 M. Hosokawa, T. Hayata, Y. Fukuda, A. Arakaki, T. Yoshino, T. Tanaka and T. Matsunaga, *Anal. Chem.*, 2010, **82**, 6629–6635.
25 L. Yang, M. Rivandi, A. Franken, M. Hieltjes, P. J. van der Zaag, C. Nelep, J. Eberhardt, S. Peter, D. Niederacher, T. Fehm and H. Neubauer, *Cytometry, Part A*, 2022, **101**, 1057–1067.
26 K. Loutherback and A. B. Dietz, *Microfluid. Nanofluid.*, 2022, **26**, 60.
27 J. R. Rettig and A. Folch, *Anal. Chem.*, 2005, **77**, 5628–5634.
28 A. Balakrishnan, D. Koppaka, A. Anand, B. Deb, G. Grenci, V. Viasnoff, E. W. Thompson, H. Gowda, R. Bhat, A. Rangarajan, J. P. Thiery, K. Govind Babu and P. Kumar, *Sci. Rep.*, 2019, **9**, 7933.
29 Bosch Healthcare Solutions GmbH, Vivalytic from Bosch, **https://www.bosch-vivalytic.com/en/tests/**, (accessed 24 April 2024).